Chemical Science

ROYAL SOCIETY OF CHEMISTRY

EDGE ARTICLE

View Article Online
View Journal | View Issue

Cite this: *Chem. Sci.*, 2021, **12**, 12429

All publication charges for this article have been paid for by the Royal Society of Chemistry

Multiple-mRNA-controlled and heat-driven drug release from gold nanocages in targeted chemo-photothermal therapy for tumors†

Hao Zhang,[a] Ze Gao,[a] Xiaoxiao Li,[a] Lu Li,*[a] Sujuan Ye*[b] and Bo Tang *[a]

Multifunctional drug delivery systems enabling effective drug delivery and comprehensive treatment are critical to successful cancer treatment. Overcoming nonspecific release and off-target effects remains challenging in precise drug delivery. Here, we design triple-interlocked drug delivery systems to perform specific cancer cell recognition, controlled drug release and effective comprehensive therapy. Gold nanocages (AuNCs) comprise a novel class of nanostructures possessing hollow interiors and porous walls. AuNCs are employed as a drug carrier and photothermal transducer due to their unique structure and photothermal properties. A smart triple-interlocked I-type DNA nanostructure is modified on the surface of the AuNCs, and molecules of the anticancer drug doxorubicin (DOX) are loaded as molecular cargo and blocked. The triple-interlocked nanostructure can be unlocked by binding with three types of tumor-related mRNAs, which act as "keys" to the triple locks, sequentially, which leads to precise drug release. Additionally, fluorescence-imaging-oriented chemical–photothermal synergistic treatment is achieved under illumination with infrared light. This drug delivery system, which combines the advantages of AuNCs and interlocked I-type DNA, successfully demonstrates effective and precise imaging, drug release and photothermal therapy. This multifunctional triple-interlocked drug delivery system could be used as a potential carrier for effective cancer-targeting comprehensive chemotherapy and photothermal therapy treatments.

Received 12th April 2021
Accepted 6th August 2021

DOI: 10.1039/d1sc02017j

rsc.li/chemical-science

Introduction

Conventional chemotherapeutic agents are still limited by their dispersibility in aqueous solution, low permeability in cell membranes, and unexpected biodistribution.[1,2] Inspiring efforts have been devoted to exploring safe and effective drug carriers for imaging, targeting therapy, and pharmacokinetic monitoring of tumors. The perfect drug carrier should exhibit specific targeting, controlled release, favorable biocompatibility properties, and the desired drug loading capacity. Nanoparticles, using both self-delivery and active targeting strategies, can enhance the intracellular concentration of drugs in cancer cells while avoiding toxicity in normal cells.[3,4] Various types of nanomaterials, such as polymeric nanoparticles,[5–7] liposomes,[8,9] carbon nanotubes,[10] metal–organic frameworks and biodegradable polymers have exhibited the desired imaging, drug loading, drug delivery and cancer therapy ability.[11,12] However, these drug carriers only provided chemotherapy for cancer treatment. A comprehensive therapeutic method has become an urgent need. A class of gold (Au) nanostructures known as nanocages (NC) have attracted considerable attention in recent years, with hollow interiors and ultrathin, porous walls.[13] AuNCs are increasingly becoming a suitable candidate for drug delivery and laser therapy owing to their excellent properties, such as their large surface area, high pore volume, tunable pore size, and biocompatible properties.[14] Moreover, AuNCs have photothermal properties based on their optical absorption, and can serve as a photothermal transducer for cancer treatment under a near-infrared laser. Additionally, AuNCs can induce the generation of reactive oxygen species from H_2O_2, such as singlet-phase oxygen and hydroxyl radicals under near-infrared excitation.[15] Xia *et al.* prepared an AuNC-modified polymer and realized photo-induced drug release with a near-infrared light trigger.[16] By combining these features, AuNCs are expected to become a new platform for cancer diagnosis and treatment.

For both diagnostic and therapeutic applications, it is critical to achieve selective drug release to increase the cellular drug uptake in cancer cells and decrease the overall dosage; thus,

[a]*College of Chemistry, Chemical Engineering and Materials Science, Collaborative Innovation Center of Functionalized Probes for Chemical Imaging in Universities of Shandong, Key Laboratory of Molecular and Nano Probes, Ministry of Education, Shandong Provincial Key Laboratory of Clean Production of Fine Chemicals, Shandong Normal University, Jinan 250014, P. R. China. E-mail: tangb@sdnu.edu.cn; lilu5252@163.com*

[b]*Key Laboratory of Optic-electric Sensing and Analytical Chemistry for Life Science, MOE, State Key Laboratory Base for Eco-chemical Engineering, College of Science and Technology, Qingdao 266042, P. R.China. E-mail: Yesujuan2010@126.com*

† Electronic supplementary information (ESI) available. See DOI: 10.1039/d1sc02017j

targeting molecules should be combined with the drug carrier. A number of ligands that selectively bind tissue-associated biomolecules (receptors) have been explored for drug delivery, including antibodies,[17] folate,[18,19] and DNA or RNA to recognize cancer markers.[20] However, most receptors of cancer cell expression often occur in normal cells as well; therefore, single ligand–receptor drug carriers potentially result in strong toxicity to normal cells, which decreases the drug efficacy and limits their biomedical applications.[21–24] Thus, multiple-ligand–receptor drug carriers for recognizing specific disease cells and enhancing diagnostic and therapeutic accuracy should be more practical and safe.[25–29] Tang reported a drug delivery system with two types of tumor-related mRNAs to induce one-drug controlled release.[20] However, no drug delivery systems have been designed for simultaneous targeting of three or more receptors in cancer cells. Such drug delivery systems with multiple ligands to synergistically control drug release could be more effective and safe.[30–33]

In this work, three types of mRNAs act as "keys" to synergistically open the multiple valves of a nanocarrier to control drug release. We designed a smart triple-interlocked I-type DNA nanostructure and modified it onto the surface of an AuNC. The AuNC can be prepared *via* the galvanic replacement reaction between silver nanocubes and chloroauric acid. Using the hollow structure of the gold NC, molecules of the anticancer drug doxorubicin (DOX) are loaded, and the I-type DNA nanostructure acts as a "triple-interlock" to lock up the AuNC carrier. An AuNC drug delivery system mediated by three types of mRNAs was developed for tumor-targeting chemotherapy and photothermal therapy. Through the binding of the I-type DNA strands, three types of tumor-related mRNAs act as "keys" to synergistically open the valve, allowing controlled drug release. Furthermore, a thermal effect is produced under illumination with infrared light. The heat generated by the infrared light pushes the remaining drugs out of the AuNC. Fluorescence imaging, drug release and photothermal therapy of the target MCF-7 cells were successfully achieved using the drug delivery system. The results of *in vivo* experiments indicate that the nanometer-scale gold cage drug carrier system can effectively treat tumors.

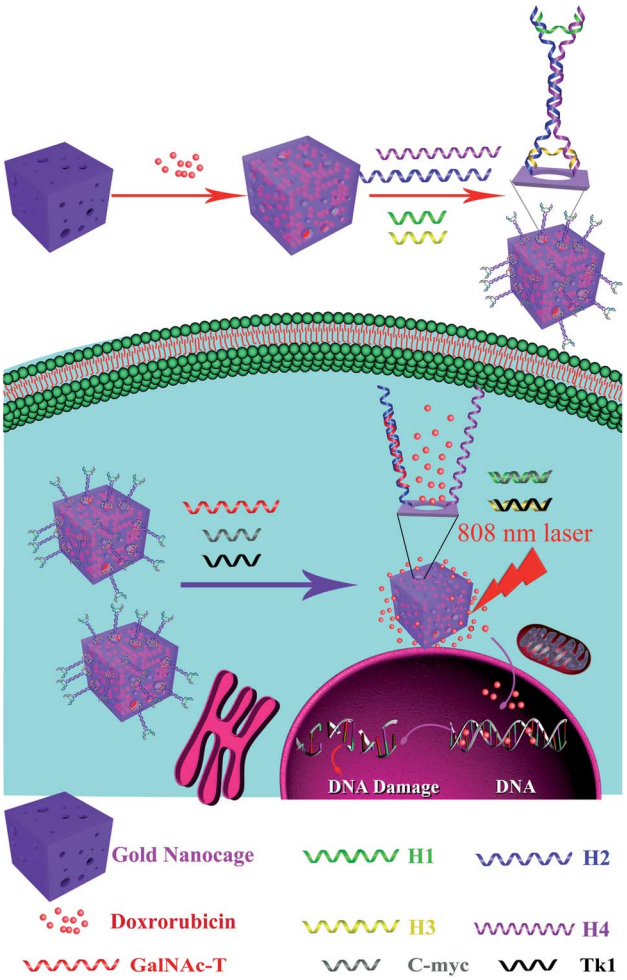

Scheme 1 Schematic illustration of the targeted drug release.

Results and discussion

Principle of the targeted drug release and photothermal therapy of I-type DNA nanostructure–AuNC

To improve the efficacy of synergistic chemical–photothermal tumor treatment, we present a multifunctional drug delivery system, which is an I-type DNA triple-interlocked AuNC for controlled drug release and photothermal therapy. The principle of this system is depicted in Scheme 1. Initially, the triple-interlocked I-type DNA nanostructure is composed of four functional DNA strands (H1–4). The H3 and H4 strands, which are terminally modified with thiol groups, are complementary to H1 and H2, resulting in the formation of an I-type structure. The complementarity between the DNA strands generated a triple-interlock that provided the recognition sites for the three keys. AuNCs were synthesized from an Ag template using a galvanic replacement reaction between solutions containing metal precursor salts and Ag nanostructures prepared through polyol reduction. The drug delivery system was synthesized by immobilizing the triple-interlocked I-type DNA scaffold on the AuNC *via* a gold–thiol bond. The anticancer drug DOX molecules were loaded as molecular cargo and blocked. MCF-7 cells were selected as a model, and three mRNAs that are specific important markers in MCF-7 cells, namely, TK1,[34] C-myc[35] and GalNAc-T,[36] were selected as the three keys. Only when C-myc, TK and GalNAc-T mRNA exist simultaneously in the system will the triple-interlock be unlocked and release DOX through competitive hybridization between DNA H1 and C-myc, H2 and TK1, and H3 and GalNAc-T. The hollow AuNC can achieve plasmon resonance absorption on both its outer and inner surfaces. It can be used as a high-performance light-to-heat conversion agent to cause tumor apoptosis *via* the heating of the AuNC under NIR irradiation. The tumor cells were effectively killed by the combination of DOX with the heated AuNC. Chemotherapy combined with photothermal therapy could be monitored in real time *via* fluorescence imaging of DOX. The multifunctional triple-interlocked drug delivery system could be used as a potential carrier for effective cancer-targeting

comprehensive chemotherapy and photothermal therapy treatment.

Characterization of the silver nanocubes (Ag nanocubes) and AuNCs

The synthesized Ag nanocubes and AuNCs were characterized using TEM and UV-visible spectroscopy, as exhibited in Fig. 1. As can be seen in Fig. 1A, the Ag nanocubes have sharp edges and angles with a uniform size; the side length is approximately 35 nm. Fig. 1B depicts their UV-visible spectrum with two distinct peaks at 355 nm (a shoulder peak) and 420 nm (the characteristic absorption peak), respectively. In Fig. 1C and D, the synthesized AuNCs have a lighter color in the middle, which proves that they are hollow inside, and the light transmittance on the walls attests to the presence of holes in the walls. The spectrum exhibits a remarkable characteristic absorbance at 728 nm, which demonstrates the successful preparation of AuNCs.

MTT experiment

The cytotoxicity of the AuNC in MCF-7 cells was tested using the MTT assay. 100 μL of MCF-7 single-cell suspension was inoculated in a culture dish and incubated in a sterile incubator for 16 h. The AuNC were dispersed into 2 mL of culture medium and incubated with the cells for approximately 6, 12, 18, or 24 h, respectively. The culture medium was then discarded, the cells were washed three times in PBS buffer, 50 μL of MTT solution was added, and the cells were continuously incubated for 4 h. Finally, 100 μL of dimethyl sulfoxide (DMSO) was added and the cells were shaken at low frequency for 10 min, after which the absorbance at a wavelength of 490 nm was measured. The data in Fig. 2 show that the AuNCs have low cytotoxicity.

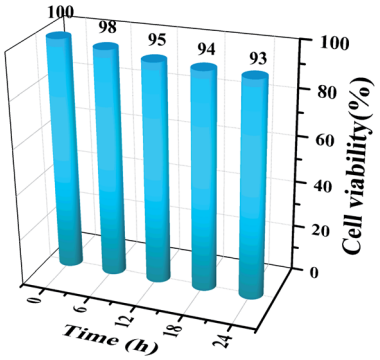

Fig. 2 MTT assay of MCF-7 cells. The cells were incubated with AuNCs for 0 h, 6 h, 12 h, 18 h and 24 h.

Characterization of the I-type DNA

To verify the hybridization of H1, H2, H3 and H4, polyacrylamide gel electrophoresis (17.5% N-PAGE) was carried out, and the results are displayed in Fig. 3. Lane a is the DNA marker, lanes b–e represent the strands H1–H4, and lane f represents the hybridized DNAs, which exhibited a new bright band, thus demonstrating the successful synthesis of I-type DNAs.

Characterization of the multifunctional drug delivery system

In order to confirm the formation of the drug carrier complex, one of the terminals of strands H1 and H2 was labeled with BHQ and Cy5, respectively, and the UV-visible spectra of all the materials were measured using a Cary 50 UV/vis-NIR spectrophotometer. In Fig. 4A, curves a–e represent the absorbance of AuNCs, DOX, Cy5-DNA (H2′), BHQ-DNA (H1′) and DNA, which exhibit characteristic absorption peaks at 728 nm, 480 nm, 640 nm, 530 nm and 260 nm, respectively. Fig. 4B is the

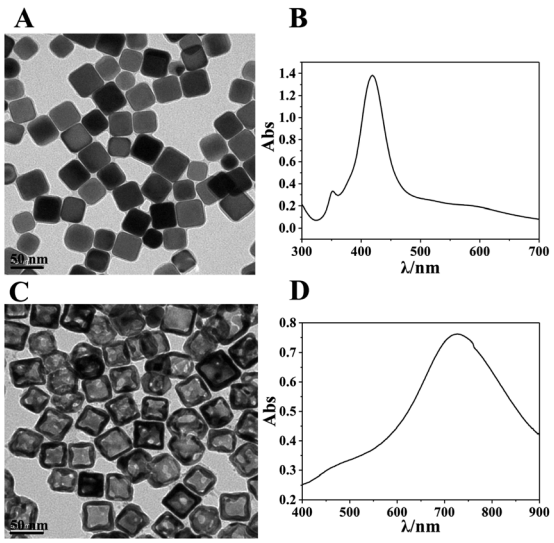

Fig. 1 (A and B) TEM images and UV spectra of the synthesised Ag nanocubes; (C and D) TEM images and UV spectra of the synthesised AuNC.

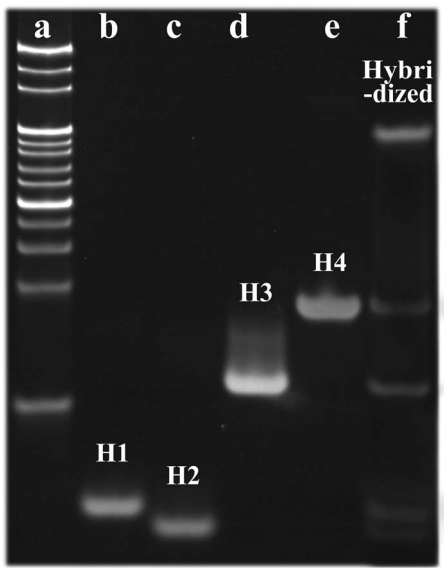

Fig. 3 Electrophoresis diagram of the DNA plugging material (a) DNA marker; (b) H1; (c) H2; (d) H3; (e) H4; (f) Hybridized DNA).

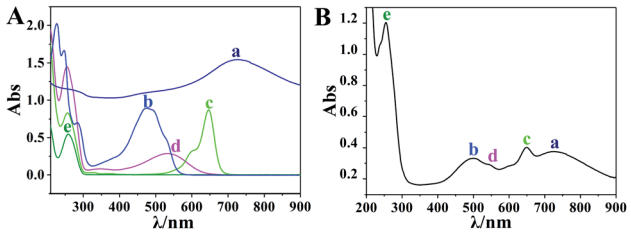

Fig. 4 (A) Ultraviolet absorption spectra of AuNC (a), DOX (b), Cy5-DNA (c), BHQ-DNA (d) and DNA (e); (B) ultraviolet absorption spectrum of the drug carrier complex.

characteristic absorbance curve of the drug–carrier complex, which corresponded to those in Fig. 4A. Thus, the drug–carrier complex formed by the I-type DNAs (the sealing material), AuNC and DOX was successfully assembled. The zeta potentials of the AuNC, AuNC/DNA and DOX@AuNC/DNA were −14.47 mV, −19.47 mV and −16.43 mV, respectively (Fig. S1†). The change in the surface charge of the particles further indicated the successful coating of the DNA nanolocks and the successful encapsulation of DOX. By measuring the fluorescence intensity of DOX in the total solution and the supernatant at its excitation and emission wavelengths of 490 nm and 590 nm, we calculated the loading capacity of the AuNC. According to the linear fluorescence calibration curve of DOX in Fig. S2,† the loading capacity of the AuNC was calculated to be 19.74 μg DOX per 1 mg AuNC. Table S1† shows that the DNA grafting count on each AuNC was 123, revealing that the DNA could be effectively assembled on the AuNC. With this adequate amount, the DNA could form an I-type structure on the surface of the AuNC. The I-type structure was sufficient and large enough to block the nanopores and prevent the leakage of DOX *via* a steric hindrance effect. To test the stability of the carrier under storage conditions, we also investigated the DOX release profile in the dark at room temperature for various times (Fig. 5B). The experimental results showed that little DOX was released before 6 h. The release of DOX was slightly increased after 6 h, but was only approximately 14% of the maximum release (Fig. 5B, line a). The result indicated that the grafting intensity was strong enough that the DOX@AuNC/DNA could be stably stored in the dark at room temperature.

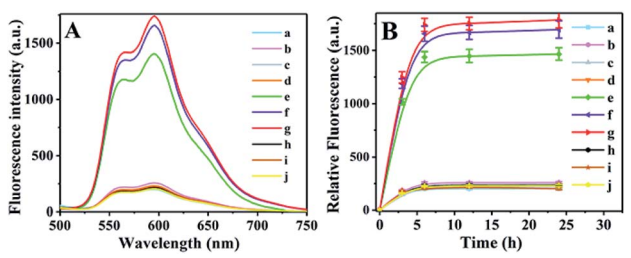

Fig. 5 (A) The fluorescence intensity of DOX (596 nm) in the supernatant under different conditions after 6 h of reaction and (B) the DOX release profile in the storage condition after different times. ((a) PBS; (b) TK1; (c) c-myc; (d) GalNAc-1; (e) TK1 + c-myc + GalNAc-1; (f) NIR; (g) TK1 + c-myc + GalNAc-1 + NIR; (h) TK1 + c-myc; (i) c-myc + GalNAc-1; (j) TK1 + GalNAc-1).

Targeted drug release assay in centrifuge tubes

The DOX@AuNC/DNA was incubated in centrifuge tubes, and the dynamic DOX release process was measured. Fig. 5A shows that little DOX was released when only one type (Fig. 5A, line b–d) or two types of mRNAs were added (Fig. 5A, line e, i and j), which indicated that the mesopores on the surface of the AuNC remained almost blocked. Only when TK1, c-myc, and GalNAc-T mRNA were all present could the drug be released from the AuNC (Fig. 5A, line e). As can be seen from line f, large quantities of DOX were released due to heat-driven diffusion under NIR irradiation. The largest release of DOX was observed for NIR irradiation and the three kinds of mRNAs (Fig. 5A, line g). The experiment verified the specificity of the multifunctional triple-interlocked drug delivery system.

To illustrate the effect of heat on drug release, we further conducted the DOX release experiment at 85 °C, 55 °C and room temperature (Fig. S3†). When the solution temperature was raised to 85 °C by NIR irradiation, the fluorescence intensity of the DNA@AuNC complex solution without target mRNAs (yellow line) was similar to that of the solution with the target mRNAs (gray line), and was as strong as that of the maximum DOX release in the DNA@AuNC complex solution with the target mRNAs irradiated by continuous high-power NIR (brown line). The results indicated that heat played a major role in DOX release through the dehybridization of locked DNA at high temperature. When a solution temperature of 55 °C was induced by NIR, the fluorescence intensity of the DNA@AuNC complex solution with the target mRNAs (light blue line) was much stronger than that of the solution without the target mRNAs (blue line), indicating that the target mRNAs played an important role in DOX release at 55 °C. In addition, the DOX release in the DNA@AuNC complex solution with the target mRNAs at 55 °C was a little higher than that of the solution with the target mRNAs at room temperature, which illustrated that the increase from room temperature to 55 °C partially contributed to the release of DOX.

Drug targeted release assay in cells

Fluorescence imaging of DOX was used to monitor the dynamic process of drug release.

The multifunctional drug delivery system was incubated in MCF-7, Hela and MCF-10A cells, and the dynamic release process of the AuNCs could be observed and imaged when TK1,[34] C-myc[35] and GalNAc-T[36] mRNA were present simultaneously. Fig. S5† shows the level of the three target mRNAs as determined by RT-PCR in the MCF-10A, MCF-7 and 4T1 cells. As shown in Fig. 6, fluorescence imaging was utilized to monitor the distribution of the AuNCs and the drug release due to the reaction between the sealing materials and mRNAs. Increasing amounts of AuNC loaded with DOX were ingested by MCF-7 cells with increasing time, and DOX could be released by the opening of the AuNC through the hybridization of the I-type DNAs with the mRNAs. Therefore, the DOX was found to be

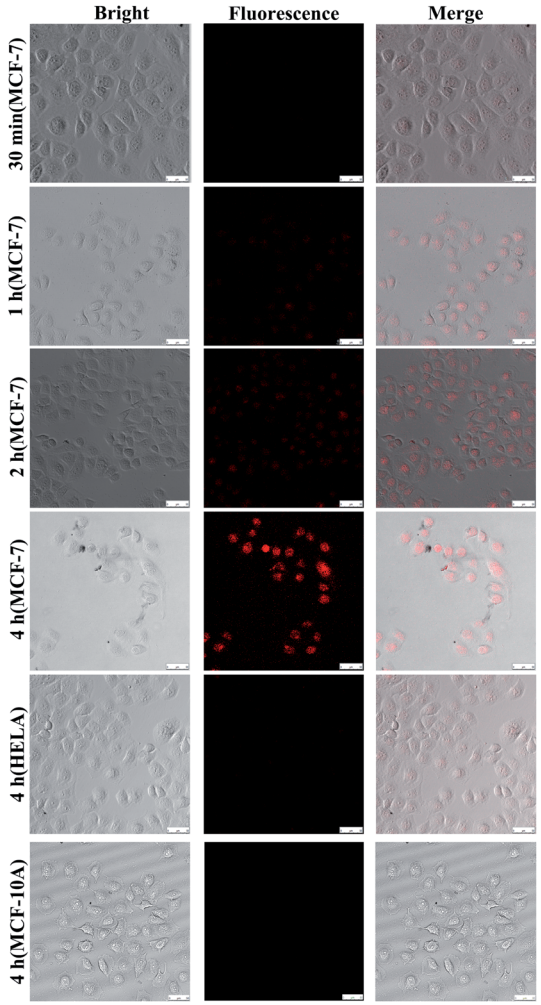

Fig. 6 Fluorescence images of drug release. The scale bar is 50 μm.

located in the cell nucleus. The fluorescence signal showed a notable increase in intensity with time from 30 min to 4 h. The fluorescence images demonstrated that the targeted release of anticancer drugs could be effectively achieved by using AuNC loaded with DOX and multiple mRNAs as a release switch. The DOX@AuNC ingested in the Hela and MCF-10A cells did not show conspicuous fluorescence due to their low expression of the C-myc, TK1 and GalNAc-T mRNAs; thus, the experiment further verified the specificity of the multifunctional triple-interlocked drug delivery system.

In vitro and *in vivo* thermal imaging

The photothermal effects of AuNCs *in vitro* and *in vivo* were observed using an infrared thermal imaging system. PBS, DOX, AuNCs, and DOX@AuNC, were placed into EP tubes for thermal imaging after NIR irradiation. The photothermal conversion ability of AuNCs in different conditions was studied under NIR light irradiation (808 nm, 1.5 W cm^{-2}). With increasing time, the temperature initially rose, and was basically stabilized after 120 s. Greater temperature changes were observed for higher concentrations of AuNCs. AuNCs at a concentration of 300 μg mL^{-1} eventually reached about 85 °C, proving that AuNCs have excellent photothermal properties. The temperature increase trends of the AuNCs before and after drug loading were then explored using an infrared temperature imaging system. Fig. 7A shows that AuNCs and DOX@AuNC have good photothermal performance; the temperatures of the samples containing AuNCs or DOX@AuNC were higher than those of the separate PBS and DOX samples. Mice with mammary tumors were treated with PBS, DOX, AuNCs, or DOX@AuNC and subsequently irradiated with an NIR laser at the tumor site. As shown in Fig. 7C, the local temperature of the tumor treated with AuNCs and DOX@AuNC was almost 55 °C, compared to a temperature of 37 °C for the tumors treated with PBS and DOX. It has been reported that cell damage is irreversible when the temperature of the heated tissue reaches a certain value (about 42 °C). To ensure that only the three kinds of mRNAs can specifically initiate DOX release and to avoid the DNA melting transition due to NIR triggered heating,[37] we carefully designed the number of complementary pairs of DNA bases to increase the melting temperature (TM). The T_m temperatures of the four DNA strands are 65.4 °C, 71.1 °C, 71.8 °C and 69.4 °C, respectively, as determined using the Oligo Calculation Tool of Thermo Fisher Scientific. In order to verify the temperature of the AuNCs at the tumor site, we conducted an *in vitro* simulation experiment. We used a piece of mouse underarm skin to cover one side of a centrifuge tube, and then irradiated the

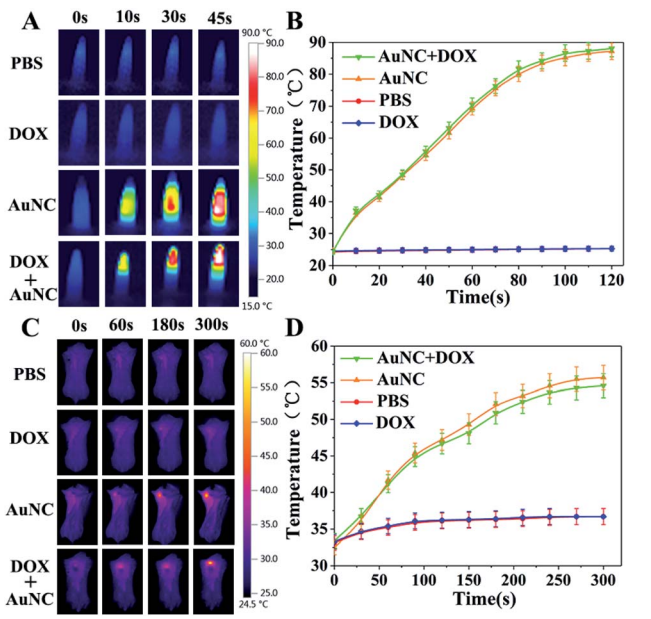

Fig. 7 *In vitro* and *in vivo* thermal imaging. (A) IR thermal images of PBS, DOX, AuNCs, and DOX@AuNC in EP tubes under 808 nm laser irradiation (1.5 W cm^{-2}) for different durations. (B) Temperature changes of PBS, DOX, AuNCs, and DOX@AuNC under NIR laser irradiation (808 nm, 1.5 W cm^{-2}). (C) *In vivo* infrared thermal (IRT) images of tumor-bearing mice during laser irradiation (808 nm, 1.5 W cm^{-2}) at 4 h post-injection of PBS, DOX, AuNCs, or DOX@AuNC and (D) temperature changes in the tumor regions during laser irradiation. The data are presented as the mean ± s.d. (n = 3). The AuNC described above were encased by I-type DNA.

centrifuge tube with a 808 nm laser and measured the temperature change of the AuNCs within. From Fig. S6† and 7D, it can be seen that the temperature of the AuNCs at the tumor site reached only 55 °C due to the energy loss of the laser as it passed through the skin.[38] The laser energy loss would lead to the reduction in the heat generated by the AuNCs. Additionally, Fig. 8 also verifies that the drug was not released *in vivo* due to thermally induced dehybridization of the DNA lock system. These results showed that the fluorescence intensity of ICG-loaded AuNCs locked by four types of random DNAs hardly changed after NIR irradiation. Based on the *in vitro* experimental data and melting temperature calculation, we could infer that it is impossible to melt the DNA chains to release DOX under NIR light irradiation *in vivo*.

Drug release assay *in vivo*

To verify the specificity of the multifunctional triple-interlocked drug delivery system, we performed a supplementary negative control experiment *in vivo*, in which AuNCs were locked by four types of random DNAs. In order to study the drug release in mice *via in vivo* fluorescence imaging, the near-infrared fluorescence probe ICG was used to replace the DOX loaded in the AuNCs. We injected the AuNCs into the mouse tumors, and then detected the fluorescence of ICG using a whole body imaging system 4 h later to study the drug release ability *in vivo*. As can be seen from Fig. 8, the fluorescence intensity of ICG locked with four types of random DNAs was lower than the fluorescence intensity of ICG locked with the I-type DNAs that were used in this experiment. This revealed that ICG was rarely released from the random-DNA-locked AuNCs because the four types of random DNAs could not be opened by the target mRNAs and further showed that the triple-interlock system was effective *in vivo*. Additionally, we detected weak ICG fluorescence for the mice administered AuNCs locked with I-types of DNAs 4 hours after injection. The fluorescence intensity of ICG increased after NIR irradiation. This also verified that the release of drugs *in vivo* is not only controlled by mRNAs, but also driven by heat. The function of the mRNAs is to induce the dehybridization of DNA lock system and release the drugs. The role of heat is to further release drugs from the AuNCs.

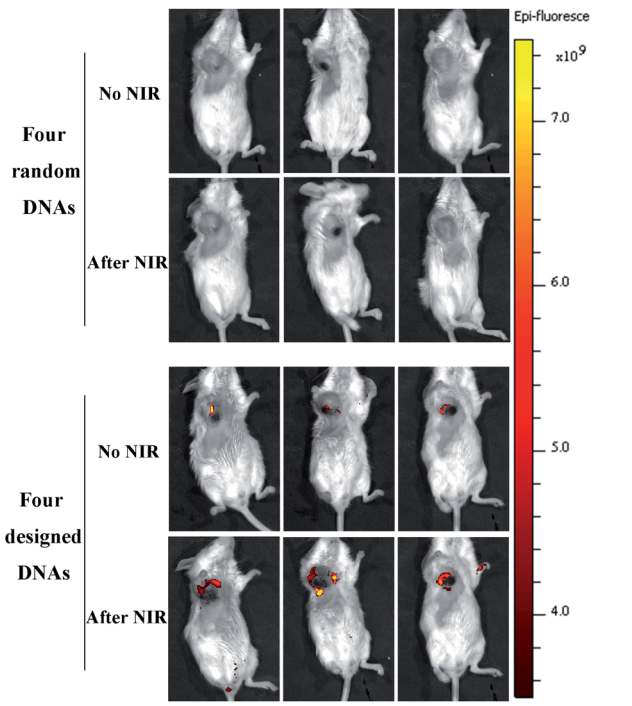

Fig. 8 *In vivo* fluorescence images of 4T1-tumor-bearing mice injected with ICG@AuNC.

Antitumor effects of DOX@AuNC *in vivo*

In order to verify the anti-tumor effect of DOX@AuNC *in vivo*, the breast cancer model mice were administered different treatments: PBS (blank control), DOX, AuNCs, AuNC + NIR, DOX@AuNC, or DOX@AuNC + NIR. Both tumor volume and mouse weight were recorded to compare the anti-tumor efficacy between groups. Fig. 9B showed that there was no significant

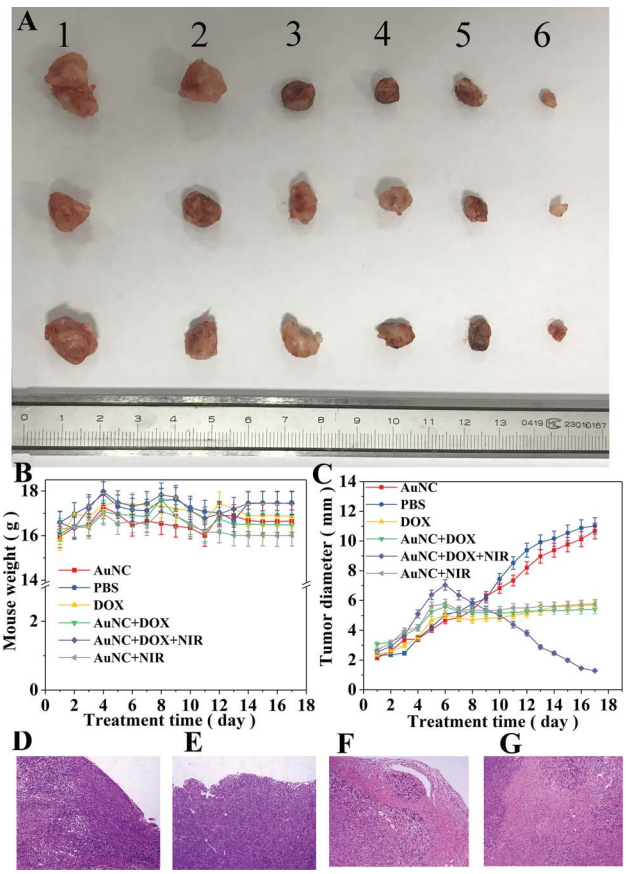

Fig. 9 *In vivo* antitumor treatment effect of DOX@AuNC. (A) Photographs of the excised tumors from the different groups (1, 2, 3, 4, 5 and 6 represent PBS, DOX, AuNCs, AuNC + NIR, DOX@AuNC, and DOX@AuNC + NIR, respectively.) (B) Body weight variation of the tumor-bearing mice during treatment. (C) Tumor growth curves of mice in the different treatment groups. The data are presented as the mean ± s.d. ($n = 3$). Histological observations to assess the apoptosis of the tumor tissues after treatment with PBS (D), DOX (E), DOX@AuNC (F) and DOX@AuNC + NIR (G). The AuNCs described above were encased by I-type DNA.

reduction in the body weights of mice treated using the various conditions, indicating that the DOX@AuNC probes have good biocompatibility and caused little damage to the bodies of the mice. As shown in Fig. 9C, AuNC injection had a small inhibitory effect on tumor volume, and the DOX group, AuNC + NIR group and DOX@AuNC group had different degrees of inhibition, with the effect of the DOX@AuNC + NIR group on tumor inhibition being the largest. Fig. S4† shows the change in the cell survival rate with increasing infrared irradiation time. The results showed that the DOX@AuNC probes we developed had a combination chemical–photothermal therapy effect, which could treat cancer more effectively.

The mice were killed at day 17, and the tumors of the mice treated under the various conditions are shown in Fig. 9A. It is obvious that the tumor volume of the DOX@AuNC + NIR group was smallest, that is, the tumor treatment effect of the DOX@AuNC + NIR group was the best. Furthermore, the tumor tissues were investigated using histological analysis after staining with hematoxylin and eosin (HE). As shown in Fig. 9, massive cell remission and high cell apoptosis occurred in the tumor treated with DOX@AuNC under NIR irradiation, confirming its synergistic effect in suppressing the tumor growth. The *in vivo* experiment results further indicated that this I-type DNA triple-interlocked AuNC presented an excellent therapeutic effect for cancer treatment. Thus, we concluded that chemical–photothermal synergistic treatment was successfully performed to treat cancer cells.

Conclusions

In summary, to improve the efficacy of synergistic chemical–photothermal tumor treatment, we have presented a multifunctional drug delivery system, I-type DNA triple-interlocked AuNCs, for mRNA-controlled and heat-driven drug release and photothermal therapy. Only when the three types of mRNAs that act as "keys" were hybridized with the respective triple-interlocks could the valves of the nanocarrier be opened, and then the drug was released into the cancer cells *via* heat-driven release, which improves the targeting of chemotherapy. A strong thermal effect was produced under illumination with infrared light, which also kills cancer cells. Thus, synergistic chemical–photothermal treatment was successfully performed to treat cancer cells. The drug release experiment indicated that the drug delivery system released DOX gradually and steadily under physiological conditions. *In vivo* experiment results further indicated that this I-type DNA triple-interlocked AuNC presented an excellent therapeutic effect for cancer treatment. The results showed that the AuNCs could be easily loaded with different drugs for the treatment of different tumors, and could bond with different highly recognized ligands of tumor markers to realize highly effective synergistic chemo–photothermal tumor treatment.

Data availability

All experimental procedures, characterization data supporting this article have been described in the manuscript and uploaded as an ESI.† Original data shown in this paper are available from the corresponding author upon reasonable request.

Author contributions

B. Tang and S. J. Ye desigend the project. L. Li coordinated the project. H. Zhang, Z. Gao and X. X. Li performed and analyzed all experiments.

Conflicts of interest

There are no conflicts to declare.

Acknowledgements

This study was performed in strict accordance with the NIH guidelines for the care and use of laboratory animals (NIH publication, 8th edition, 2011) and was approved by the Ethics Committee of Shandong Normal University, Jinan, P. R. China (approval number AEECSDNU 2021049). This work was supported by the National Natural Science Foundation of China (21927811, 21775081, 91859111), the Natural Science Foundation of Shandong Province of China (ZR2019JQ06), the Taishan Scholars Program of Shandong Province (tsqn.201909077) and Shandong Provincial Key Research and Development Program (2019GSF107024).

Notes and references

1 E. Merisko-Liversidge, P. Sarpotdar, J. Bruno, S. Hajj, L. Wei, N. Peltier, J. Rake, J. M. Shaw, S. Pugh, L. Polin, J. Jones, T. Corbett, E. Cooper and G. G. Liversidge, *Pharm. Res.*, 1996, **13**, 272–278.
2 Y. Li, Y. Z. Shu, M. W. Liang, X. L. Xie, X. Y. Jiao, X. Wang and B. Tang, *Angew. Chem., Int. Ed.*, 2018, **57**, 12415–12419.
3 Z. Poon, D. Chang, X. Zhao and P. T. Hammond, *ACS Nano*, 2011, **5**, 4284–4292.
4 L. Xiao, L. Huang, F. Moingeon, M. Gauthier and G. Yang, *Biomacromolecules*, 2017, **18**, 2711–2722.
5 X. X. Wang, M. Qiu, C. Deng, R. Cheng and Z. Y. Zhong, *ACS Biomater. Sci. Eng.*, 2020, **6**, 2621–2629.
6 Z. T. Cao, L. Q. Gan, W. Jiang, J. L. Wang, H. B. Zhang, Y. Zhang, Y. C. Wang, X. Z. Yang, M. H. Xiong and J. Wang, *ACS Nano*, 2020, **14**, 3563–3575.
7 T. Y. Wang and C. Y. Chen, *ACS Appl. Bio Mater.*, 2019, **2**, 3659–3667.
8 E. Nogueira, A. C. Gomes, A. Preto and A. Cavaco-Paulo, *Colloids Surf., B*, 2015, **136**, 514–526.
9 K. Yokoyama, C. D. Catalfamo and M. Yuan, *AIMS Biophys.*, 2015, **2**, 649–665.
10 Z. Liu, S. Tabakman, K. Welsher and H. Dai, *Nano Res.*, 2009, **2**, 85–120.
11 B. Singco, L. H. Liu, Y. T. Chen, Y. H. Shih, H. Y. Huang and C. H. Lin, *Microporous Mesoporous Mater.*, 2016, **223**, 254–260.

12 S. S. Mano, K. Uto, T. Aoyagi and M. Ebara, *AIMS Mater. Sci.*, 2016, **3**, 66–82.
13 Y. N. Xia, W. Y. Li, C. M. Cobley, J. Y. Chen, X. H. Xia, Q. Zhang, M. X. Yang, E. C. Cho and P. K. Brown, *Acc. Chem. Res.*, 2011, **44**, 914–924.
14 Y. L. Feng, Y. Cheng, Y. Chang, H. Jian, R. X. Zheng, X. Q. Wu, K. Q. Xu, L. Wang, X. M. Ma, X. Li and H. Y. Zhang, *Biomaterials*, 2019, **217**, 119327.
15 R. J. Liang, L. L. Liu, H. M. He, Z. K. Chen, Z. Q. Han, Z. Y. Luo, Z. H. Wu, M. B. Zheng, Y. F. Ma and L. T. Cai, *Biomaterials*, 2018, **177**, 149–160.
16 S. Shen, C. L. Zhu, D. Huo, M. X. Yang, J. J. Xue and Y. N. Xia, *Angew. Chem., Int. Ed.*, 2017, **56**, 8801–8804.
17 Z. W. Su, Z. C. Xiao, J. S. Huang, Y. Wang, Y. C. An, H. Xiao, Y. Peng, P. F. Pang, S. S. Han, K. S. Zhu and X. T. Shuai, *ACS Appl. Mater. Interfaces*, 2021, **13**, 12845–12856.
18 Z. Zheng, Z. F. Li, C. C. Xu, B. Guo and P. X. Guo, *J. Control. Release*, 2019, **311**, 43–49.
19 H. Wang, T. H. Ding, J. Guan, X. Liu, J. Wang, P. P. Jin, S. X. Hou, W. Y. Lu, J. Qian, W. P. Wang and C. Y. Zhan, *ACS Nano*, 2020, **14**, 14779–14789.
20 Y. H. Li, Y. Y. Chen, W. Pan, Z. Z. Yu, L. M. Yang, H. Y. Wang, N. Li and B. Tang, *Nanoscale*, 2017, **9**, 17318–17324.
21 M. M. Attwood, J. Jonsson, M. Rask-Andersen and H. B. Schiöth, *Nat. Rev. Drug Discovery*, 2020, **19**, 695–710.
22 L. W. He, X. L. Yang, K. X. Xu, X. Q. Kong and W. Y. Lin, *Chem. Sci.*, 2017, **8**, 6257–6265.
23 X. Y. Jiao, Y. S. Xiao, Y. Li, M. W. Liang, X. L. Xie, X. Wang and B. Tang, *Anal. Chem.*, 2018, **90**, 7510–7516.
24 D. J. Yoon, C. T. Liu, D. S. Quinlan, P. M. Nafisi and D. T. Kamei, *Ann. Biomed. Eng.*, 2011, **39**, 1235–1251.
25 X. Wang, J. Sun, W. H. Zhang, X. X. Ma, J. Z. Lv and B. Tang, *Chem. Sci.*, 2013, **4**, 2551–2556.
26 G. D. Yang, L. Y. Wu, B. Jiang, W. Yang, J. S. Qi, K. Cao, Q. H. Meng, A. K. Mustafa, W. T. Mu, S. M. Zhang, S. H. Snyder and R. Wang, *Science*, 2008, **322**, 587–590.
27 H. Li and M. Q. Zhong, *Med. Res. Rev.*, 2020, **22**, 225–250.
28 S. P. Vyas, A. Singh and V. Sihorkar, *Crit. Rev. Ther. Drug Carrier Syst.*, 2001, **18**, 1–76.
29 G. X. Yin, T. T. Niu, Y. B. Gan, T. Yu, P. Yin, H. M. Chen, Y. Y. Zhang, H. T. Li and S. Z. Yao, *Angew. Chem., Int. Ed.*, 2018, **57**, 4991–4994.
30 J. An, S. J. Geib and N. L. Rosi, *J. Am. Chem. Soc.*, 2009, **131**, 8376–8377.
31 J. Chen, X. B. Yang, L. Q. Huang, H. X. Lai, C. H. Gan and X. T. Luo, *Drug Delivery*, 2018, **25**, 1932–1942.
32 S. C. Park, Y. M. Kim, J. K. Lee, N. H. Kim, E. J. Kim, H. Heo, M. Y. Lee, J. R. Lee and M. K. Jang, *J. Control. Release*, 2017, **256**, 46–55.
33 Z. L. Chai, D. N. Ran, L. W. Lu, C. Y. Zhan, H. T. Ruan, X. F. Hu, C. Xie, K. Jiang, J. Y. Li, J. F. Zhou, J. Wang, Y. Y. Zhang, R. H. Fang, L. F. Zhang and W. Y. Lu, *ACS Nano*, 2019, **13**, 5591–5601.
34 F. Othman, G. Motalleb, S. Lam-Tsuey-Peng, A. Rahmat, R. Basri and C. Pei-Pei, *Cell J.*, 2012, **14**, 53–60.
35 N. Li, C. Y. Chang, W. Pan and B. Tang, *Angew. Chem., Int. Ed.*, 2012, **51**, 7426–7430.
36 D. J. Gill, K. M. Tham, J. Chia, S. C. Wang, C. Steentoft, H. Clausen, E. A. Bard-Chapeau and F. A. Bard, *Proc. Natl. Acad. Sci.*, 2013, **110**, E3152–E3161.
37 K. L. Young, A. W. Scott, L. L. Hao, S. E. Mirkin, G. L. Liu and C. A. Mirkin, *Nano Lett.*, 2012, **12**, 3867–3871.
38 C. R. Simpson, M. Kohl, M. Essenpreis and M. Cope, *Phys. Med. Biol.*, 1998, **43**, 2465–2478.